CHAPTER IV
RESULTS AND DISCUSSION

4.1 Catalyst Characterization

BET, SEM, XRD, TPR, and TPD of oxygen and methanol were carried out on all of the mono-and bimetallic catalysts. The experimental results are discussed in this chapter.
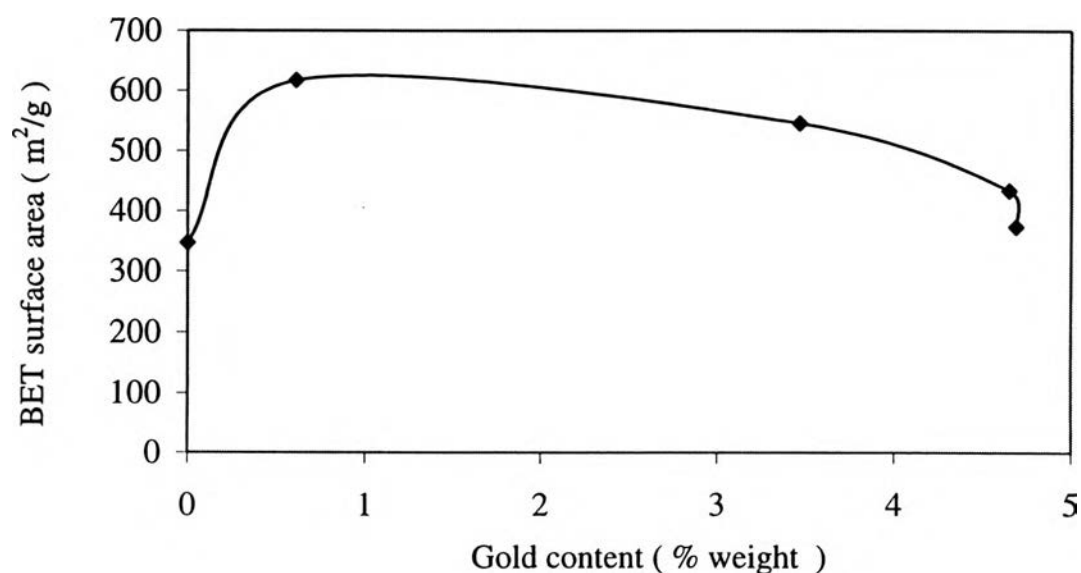
4.1.1 BET Surface Area

The BET results of the silica-supported mono-and bimetallic catalysts are shown in Table 4.1. Figures 4.1 and 4.2 show the BET surface area as a function of gold content by weight percent and atomic percent, respectively. It can be seen clearly that the addition of either pure ruthenium or pure gold resulted in a significant reduction in the BET surface area in comparison to the surface area of the blank SiO_2. However, if both ruthenium and gold were added together, the BET surface area increased remarkably when compared to either pure ruthenium or gold. The relationship between both metal contents and the BET surface area is not linear. The RS091 sample (Ru-Au/SiO_2 with 91 % atom of Ru) gives the maximum value of the BET surface area which is slightly higher than the value of the blank SiO_2. Again, the surface area of all Ru-Au bimetallic catalysts was higher than those of the monometallic catalysts. It can be explained by the work of Dayte *et al.*(1984). Based on X-ray energy dispersive spectroscopy (EDS) analysis of particles, it was found that ruthenium and gold formed bimetallic clusters in RS014, RS048, and RS091. Their particle sizes were smaller than 1 nm. It did not occur in

RS000 and RS100. Therefore, the formation of tiny particle directly resulted in increasing the surface area.

Table 4.1 Chemical composition and BET surface area of the mono-and bimetallic Ru-Au catalysts on silica support

Catalyst sample	Ru (wt %)	Au (wt %)	BET surface area (m^2/g)
SiO_2	-	-	607.6
RS100	3.86	-	346.6
Ru/SiO_2	1.00	-	613.9
RS091	3.32	0.61	617.3
RS048	1.66	3.47	546.2
RS014	0.39	4.65	434.1
RS000	-	4.69	374.4

Figure 4.1 The BET surface area of the bimetallic Ru-Au/SiO$_2$ as a function of Au content by weight percent of the total weight
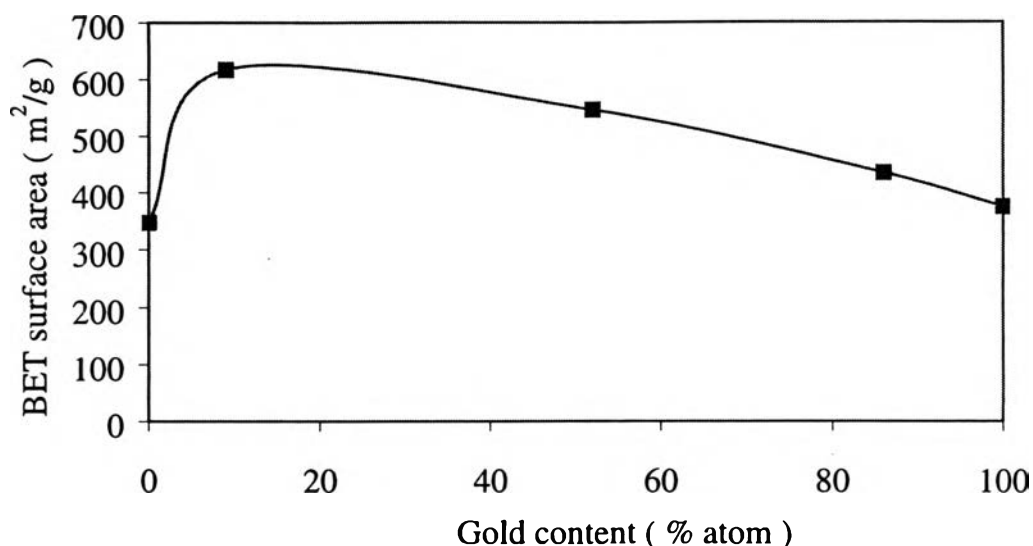
Figure 4.2 The BET surface area of the bimetallic Ru-Au/SiO$_2$ as a function of Au content by atomic percent of the metal content

The BET results of the different supports of ruthenium catalysts were shown in Table 4.2. The metal content on each support was about 1% by weight. The surface areas of Ru-Au/η-Al$_2$O$_3$ and Ru/η-Al$_2$O$_3$ were not so much different. The bimetallic clusters might not be formed on the η-Al$_2$O$_3$ support. However, the monometallic silica-supported ruthenium catalyst (Ru/SiO$_2$) had the maximum value of the surface area that was much higher than that of RS100 (Table 4.1). This can be explained that they had the different ruthenium content on the silica support. The surface area of ruthenium was less than that of silica (Galvagno *et al.*, 1981). Therefore, the more the ruthenium content, the less the surface area of the catalyst. For the ruthenium supported on the silica-alumina, the surface area was in the middle value between those of the ruthenium supported on silica and alumina. This implies that the interaction between silica and alumina did not modify the surface area of the catalyst.

Table 4.2 BET surface area of the bimetallic catalysts Ru-Au on the different supports at the metal content of about 1 % wt

| Catalyst sample	BET surface area (m^2/g)
Ru-Au/η-Al$_2$O$_3$	241.1
Ru/η-Al$_2$O$_3$	236.0
Ru/γ-Al$_2$O$_3$	252.7
Ru/SiO$_2$-Al$_2$O$_3$	399.8
Ru/SiO$_2$	613.9

4.1.2 Morphology of Catalysts

SEM micrographs of all silica-supported catalysts studied are shown in Figures 4.3-4.8. It is interesting that the morphology of the support changes in both size and shape when metal particles are impregnated. It was also obviously found that the averaged support particle sizes of the bimetallic catalysts, RS014, RS048, and RS091, were much smaller than that of the monometallic catalysts, RS000 and RS100. The formation of bimetallic clusters might lead to the formation of small support particles. Moreover, the SEM micrographs of these bimetallic catalysts looked very much the same. The tiny particles of the bimetallic catalysts result in having surface areas much higher than those of the monometallic catalysts have. Figures 4.9-4.12 show the differences in the morphology of two types of supports of alumina and silica. The SEM micrograph of Ru-Au/η-Al$_2$O$_3$, and Ru/η-Al$_2$O$_3$ were not different. These agreed with the result of BET surface area that Au did not affect Ru in the bimetallic formation. The shape of the particle size of the silica-supported ruthenium catalysts was different from that of the alumina supported ruthenium catalysts, which exhibited a more spherical shape. This
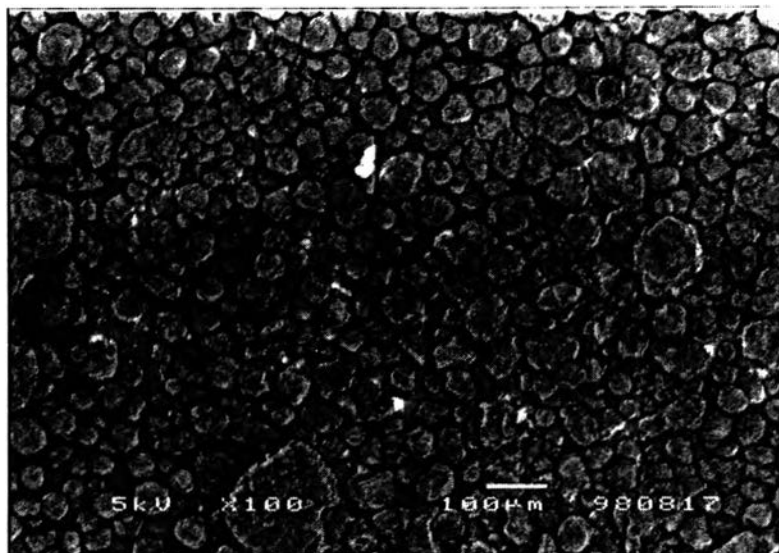
agreed with the BET results that surface area of the alumina-supported less than that of silica-supported catalysts.
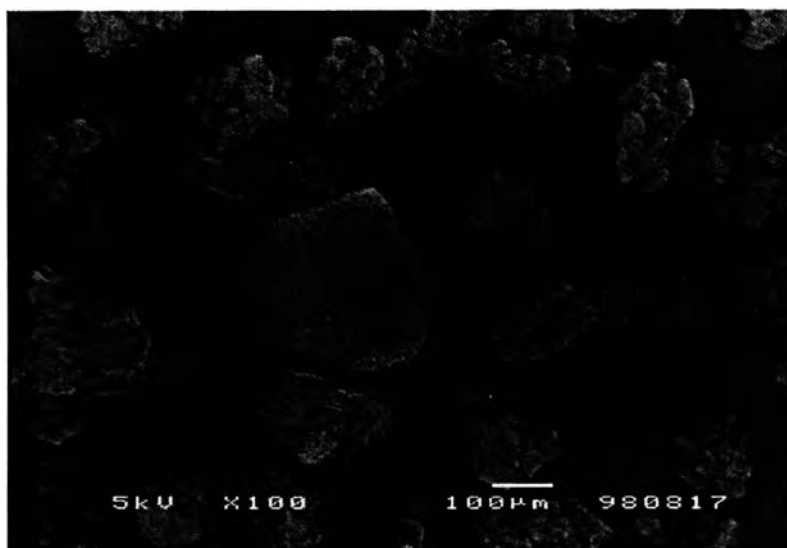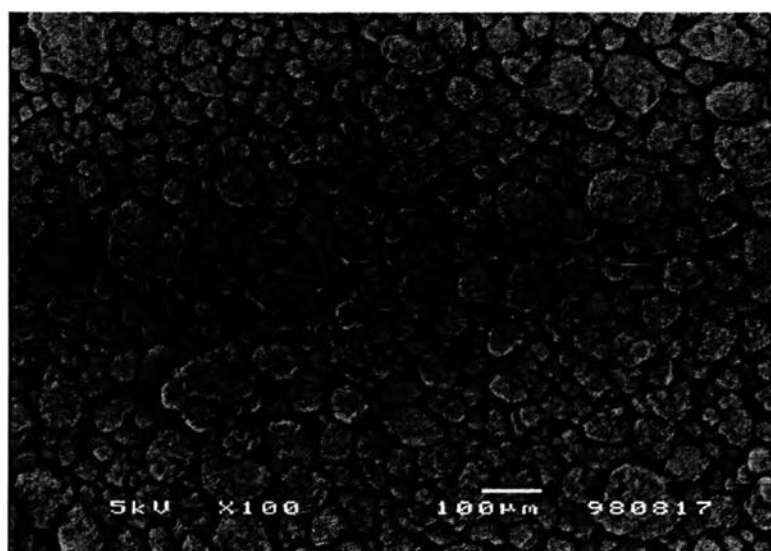

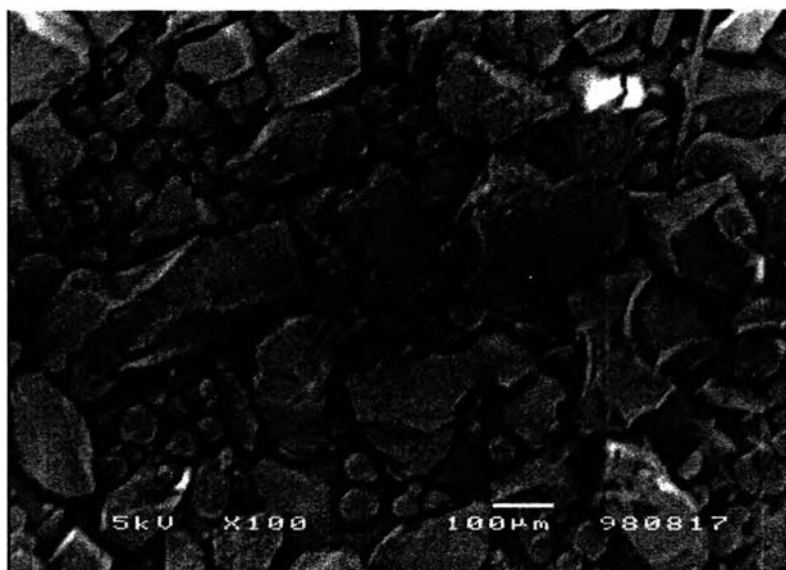**Figure 4.3 SEM micrograph of RS000 (4.69 % wt Au/SiO$_2$)**
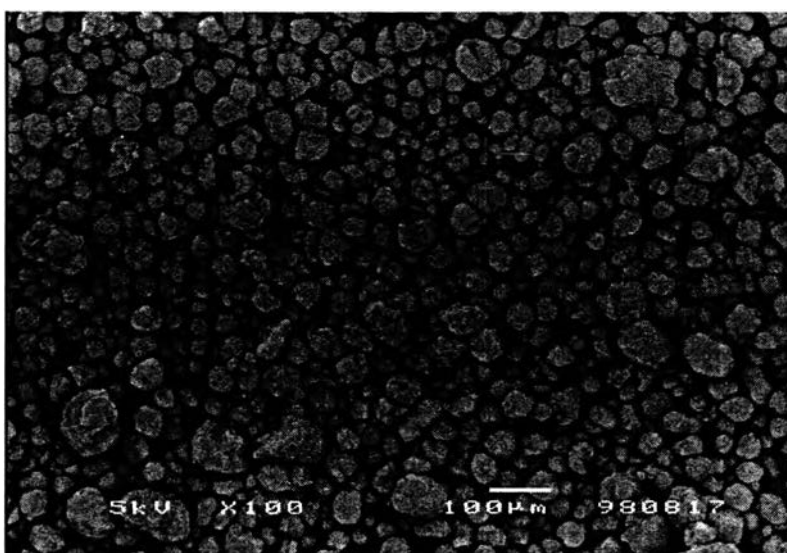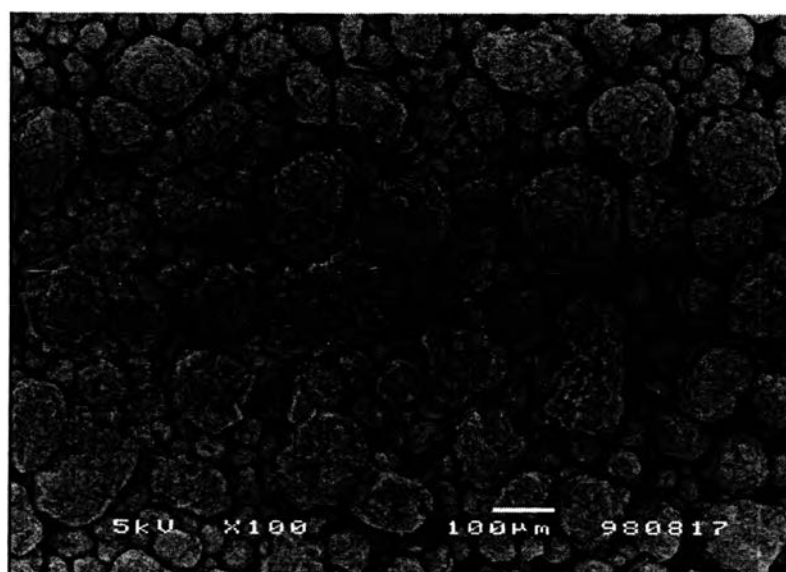

Figure 4.4 SEM micrograph of RS014 (Ru-Au/SiO$_2$)

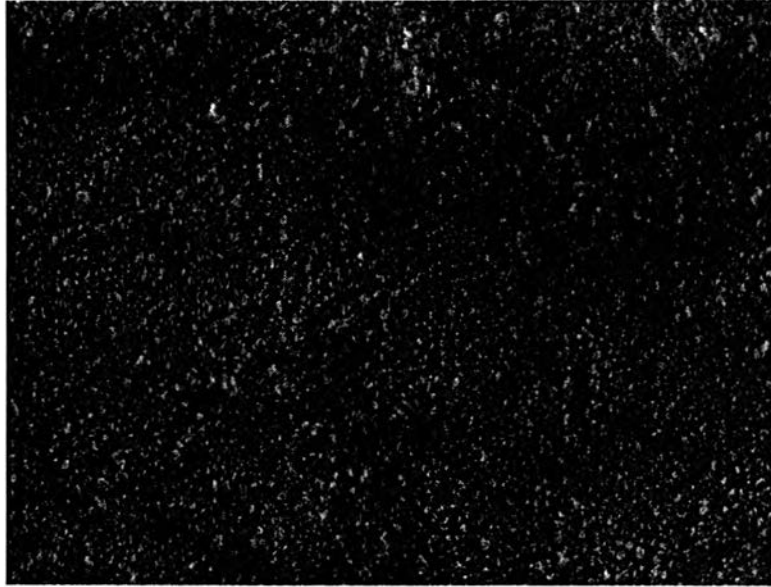**Figure 4.5 SEM micrograph of RS048 (Ru-Au/SiO$_2$)**

Figure 4.6 SEM micrograph of RS091 (Ru-Au/SiO$_2$)
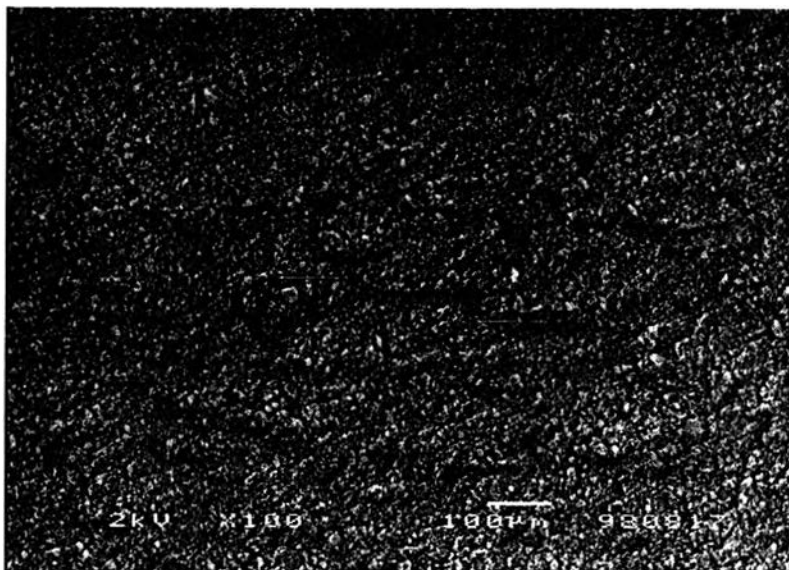
Figure 4.7 SEM micrograph of RS100 (3.86 % wt Ru/SiO₂)

Figure 4.8 SEM micrograph of silica support (Davison 951 N)
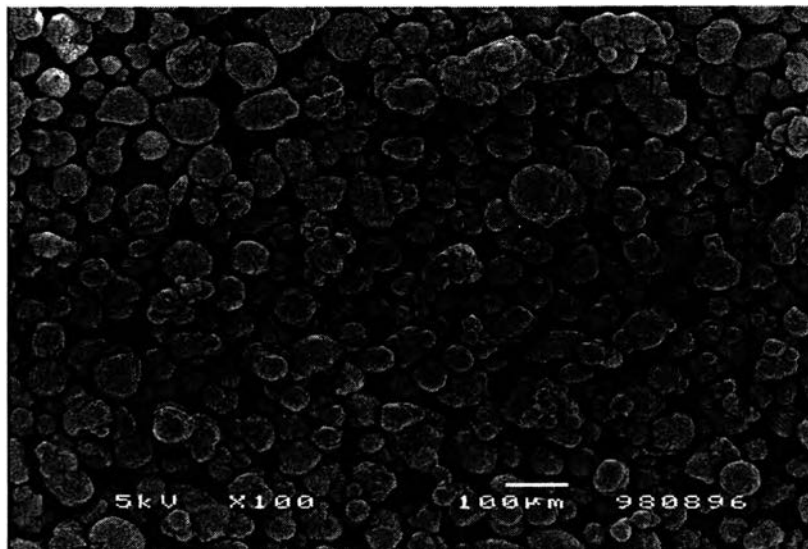
I19584684

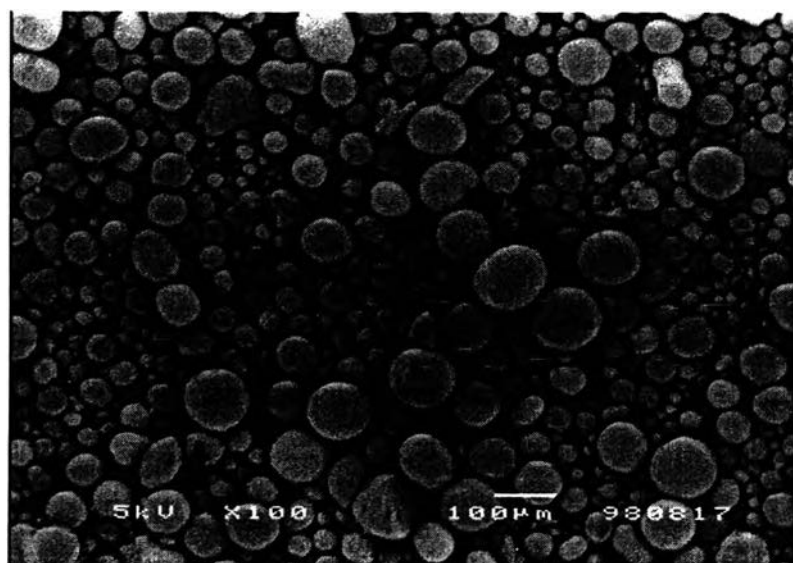Figure 4.9 SEM micrograph of 0.7 % wt Ru-Au/η-Al$_2$O$_3$

Figure 4.10 SEM micrograph of 0.7 % wt Ru/η-Al$_2$O$_3$

Figure 4.11 SEM micrograph of 1 % wt Ru/SiO₂

Figure 4.12 SEM micrograph of 1 % wt. Ru/γ-Al₂O₃

4.1.3 X-ray Diffraction Analysis (XRD)

X-ray diffraction analysis was carried out on all catalysts. The XRD patterns for a series of ruthenium-gold catalysts including pure silica support are shown in Figure 4.13. The broad peak at around $22°(2\theta)$ was corresponding to the peak of silicon oxide because it was only one peak found in the pure silica support and also from the tabulations of reference patterns. This peak was found in all catalysts supported on silica. It is confirmed by the shape of peak indicating the amorphous structure of the silica support. The XRD pattern for pure ruthenium on silica support (RS100) was not different from the pure silica support. No crystal of ruthenium was detected. This can indicate that either no crystallite of ruthenium form is present in the catalyst or the crystallites are too small to be detected by this method or else the ruthenium patterns are superimposed upon those of the other peaks. The last case might be true because from the reference files, substances composing ruthenium element show the peak at around $22°(2\theta)$. The sharp peaks at about 38, 44, 65, 78, and $82°(2\theta)$ were found in RS014, RS048, and RS091 composing of gold element. This is also confirmed by the XRD reference pattern of gold synthesis which has the sharp peaks at same diffraction angles (2θ). When the gold content was increased, the intensity of each peaks was increased significantly. The small gold content in RS091 might be not enough to show the peaks at 65, 78, and $82°(2\theta)$ in the XRD pattern. However, for pure gold supported on silica (RS000), the intensity of each peaks was not the maximum value compared to that of RS014, RS048, and RS091. If all 5 peaks mentioned above is the peak of pure gold, the intensity of each peak for RS000 should be the maximum value. Therefore, they are not the peak of pure gold. They might be the peak of the species deriving from gold and ruthenium element. This species increased when the gold content was increased in RS091, RS048, and RS014 respectively. This is because gold
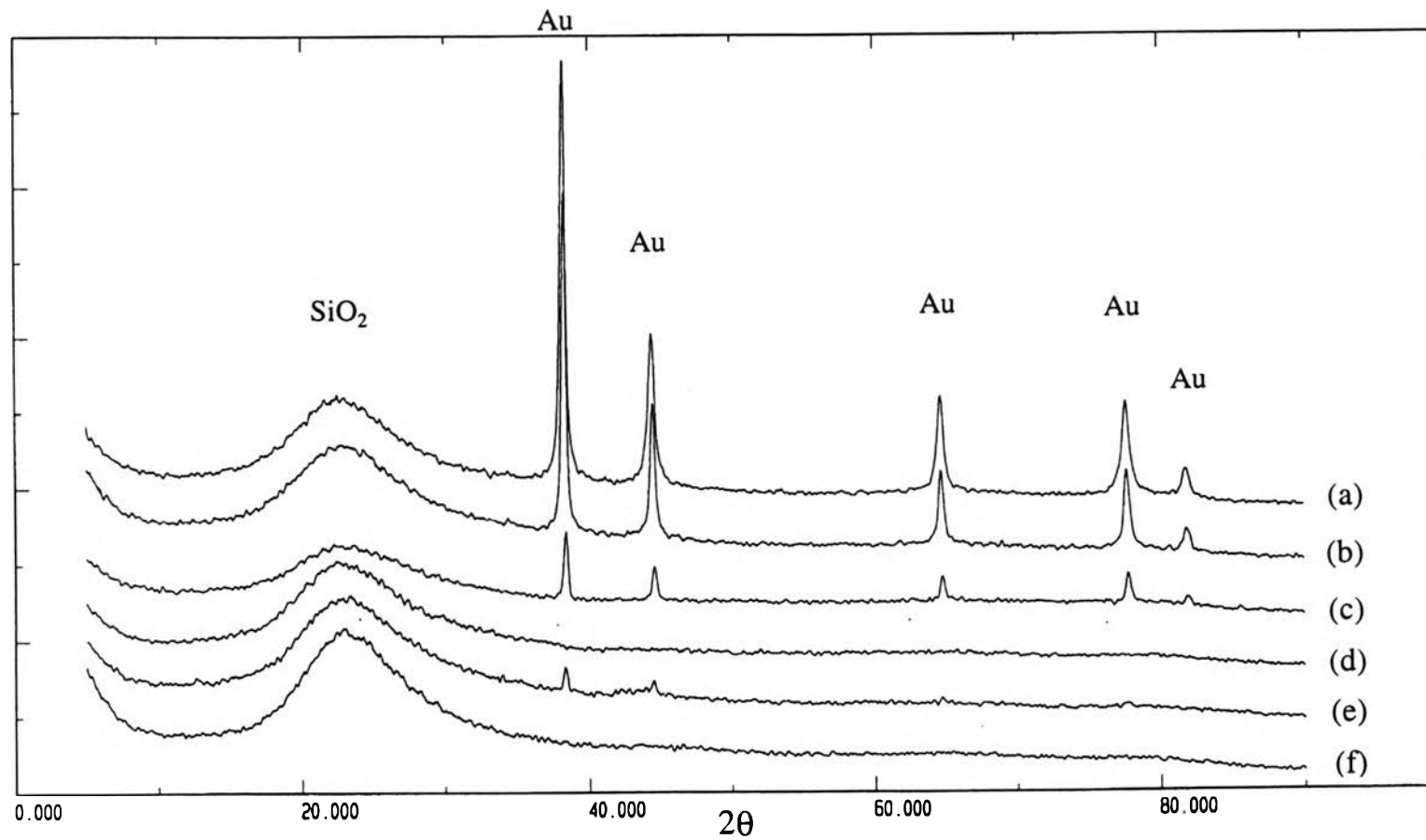
Figure 4.13 XRD patterns of (a) RS014 (b) RS048 (c) RS000 (d) RS100 (e) RS091 and (f) Davison 951N silica

characteristics was dominant than ruthenium characteristics. So those peaks were found at the same diffraction angle of gold element. The bimetallic species may be ruthenium deposited on the gold particle. This was confirmed by the work of Dayte *et al.* (1984). They found that gold particle size was larger than ruthenium particle size. This agreed with the sharp peak of gold element because the crystallite size is inversely proportional to the peak width. As the crystals get smaller and smaller, the XRD peaks get broader and broader and eventually are undetectable above the background such as ruthenium element.

The XRD patterns for the different support ruthenium catalysts are shown in Figure 4.14. The XRD patterns for Ru/η-Al$_2$O$_3$ looked similar to that of Ru-Au/η-Al$_2$O$_3$. They were mainly the aluminum oxide patterns. Crystals of gold was superimposed upon those of aluminum oxide. As the little peaks of gold crystal were detected at the tail of the aluminum oxide at 38, 44, 65, and 78°(2θ) for Ru-Au/η-Al$_2$O$_3$. They were not detected for Ru/η-Al$_2$O$_3$. Ruthenium also can not be detected on these supports by this method. From the XRD pattern of Ru/SiO$_2$-Al$_2$O$_3$, the broad peak at 25°(2θ) was only detected. From the reference files, it might be aluminum ruthenium or aluminum silicate which have the peak at around the same diffraction angle. The XRD signal of ruthenium might be superimposed up on those of silica or alumina so it shows one broad peak at 25°(2θ). The XRD pattern was similar to that of RS100 but the peak of Ru/ SiO$_2$-Al$_2$O$_3$ was broader and shifted to 25 °(2θ) while the broad peak of RS100 was at 22°(2θ). This agreed with the SEM micrograph that the particle size of Ru/SiO$_2$-Al$_2$O$_3$ was smaller than that of Ru/SiO$_2$ (RS100). As ruthenium supported on alumina, it shows a lot of crystalline plane such as pattern (a), (b), and (d) in contrast to ruthenium supported on silica which shows only one broad peak as amorphous material. Ruthenium supported on SiO$_2$ was more amorphous than that either on η-Al$_2$O$_3$ and γ-Al$_2$O$_3$ because the crystallites of Ru/SiO$_2$ were small and a well
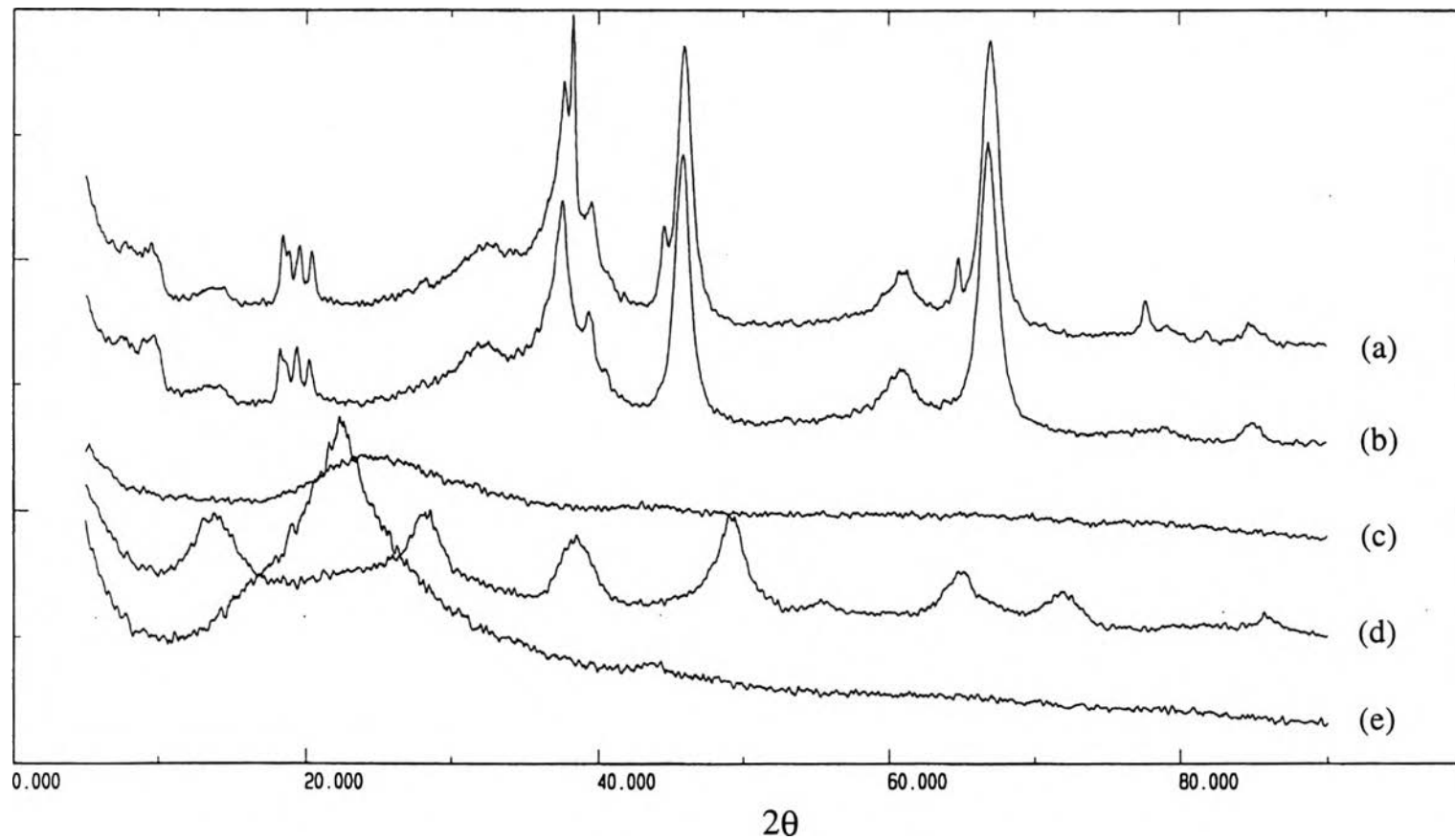
Figure 4.14 XRD patterns of (a) Ru-Au/η-Al$_2$O$_3$ (b) Ru/η-Al$_2$O$_3$ (c) Ru/SiO$_2$-Al$_2$O$_3$ (d) Ru/γ-Al$_2$O$_3$ (e) 1%wt Ru/SiO$_2$

41

defined X-ray pattern was not obtained. Materials with very small crystallites are more precisely called amorphous since they possess no long-range order to diffract X-rays (Heck *et al.*, 1995). In addition, SiO_2 was dominant Al_2O_3 in a SiO_2-Al_2O_3 material because ruthenium supported on SiO_2-Al_2O_3 was highly amorphous. Since ruthenium supported on silica shows smaller crystals than that on Al_2O_3, this agreed with the BET results that the surface area of Ru/SiO_2 was higher than that of Ru/η-Al_2O_3 and Ru/γ-Al_2O_3.

4.1.4 Temperature-Programmed Methods

The TPD profiles for methyl alcohol and oxygen were obtained for a series of ruthenium and ruthenium-gold catalysts with varying gold content supported on silica and on alumina. In addition, the TPR profiles for each catalysts were also carried out with and without oxygen pretreatment.

(a) TPD Profile of Methyl Alcohol

Figure 4.15 shows TPD profiles of methyl alcohol on a series of ruthenium-gold catalysts supported on silica. There was more than one peak in most of catalyst samples so methyl alcohol might decompose into several substances. The different substances desorbed at different temperature, leading to the appearance of several desorption peaks. The TPD pattern of pure silica support was similar to that of RS000 (Au/SiO_2). There were only two peaks at about 370 K and the broad peak starting at 723 K. It can be concluded that gold does not influence the desorption of methyl alcohol on silica support. By contrast, for both pure ruthenium supported on silica, RS100, and ruthenium metal, several small peaks were observed over the wide range of temperatures. The results indicate that ruthenium is very active with regard to methyl alcohol. When it was exposes to methyl alcohol, it decomposes and desorbs at
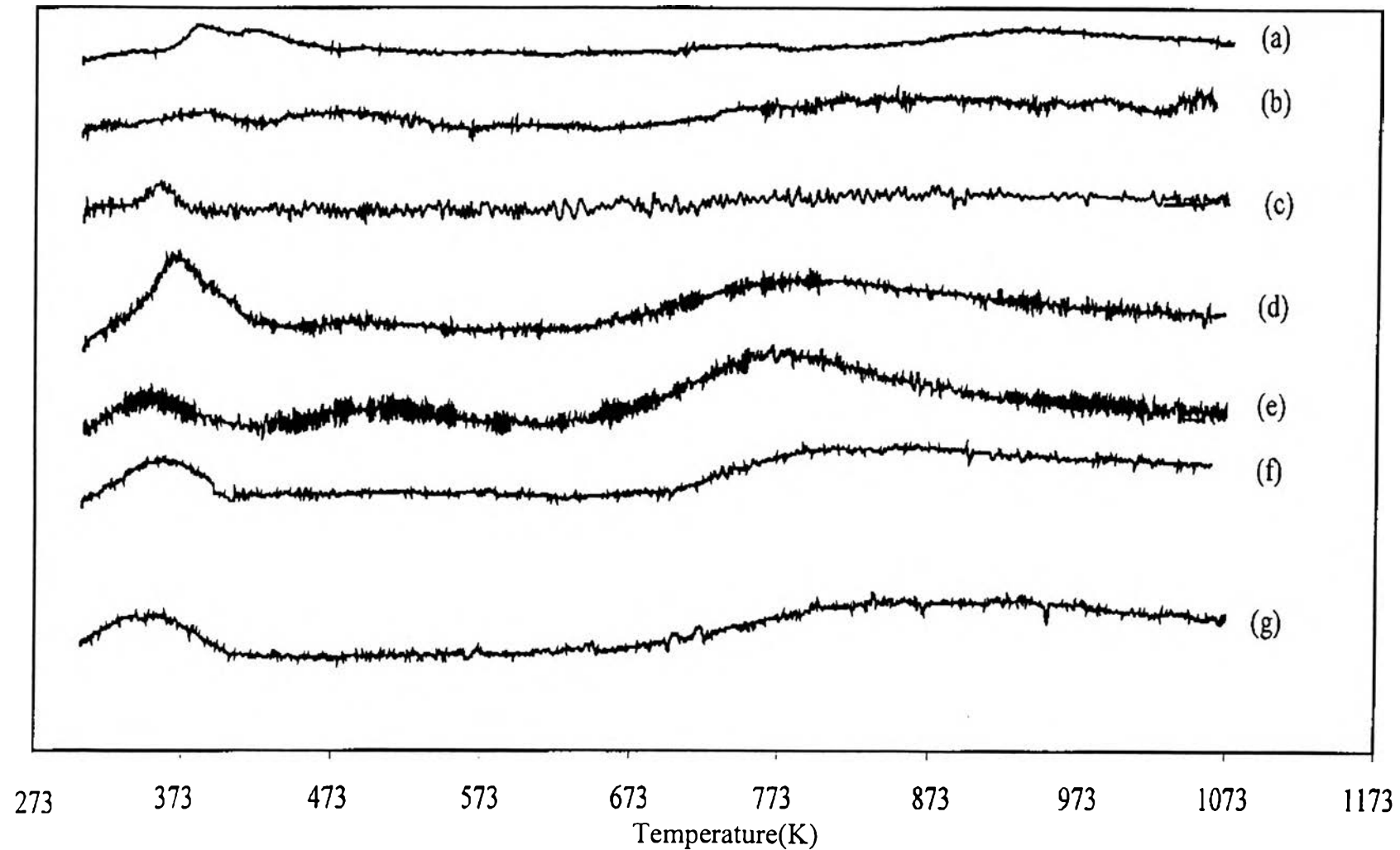
Figure 4.15 Temperature-programmed desorption of methanol on (a)Ru metal (b)RS100 (c)RS091 (d)RS048 (e)RS014 (f)RS000 (g)SiO$_2$

all range of temperatures. For RS014 and RS048, there were three desorption peaks on both catalysts at 370 K, 518 K, and 773 K. The second desorption peak at 518 K was not very pronounced on RS048 and there was only one desorption peak at 370 K for RS091. It is interesting to point out that gold had a strong effect on the desorption product of methyl alcohol when it incorporated with ruthenium metal as bimetallic catalysts. Moreover, the desorption products depended on the gold and ruthenium contents in the bimetallic catalysts. It may be explained that gold had an interaction with ruthenium leading to the different desorption products of methyl alcohol on these bimetallic catalysts. It was reported that methyl alcohol desorbed at the lower temperature than the decomposition products such as carbon monoxide, carbon dioxide, and hydrogen(Cordi and Falconer, 1996). However, they observed TPD of methyl alcohol on the catalysts different from this work. It can be noted that gold might had some effect on the ruthenium active sites causing methyl alcohol to desorb at different temperatures.

Figure 4.16 shows the TPD of methyl alcohol on ruthenium catalysts with different supports. Methyl alcohol desorbed in a single peak at 483 K on Ru/η-Al_2O_3. For Ru/SiO_2-Al_2O_3, methyl alcohol still desorbed at 483 K but gave an additional peak at 770 K. This small peak was the desorption of another different desorption product from the decomposition of methyl alcohol. The peak of desorption of methyl alcohol was slightly shifted to 500 K on Ru/γ-Al_2O_3 and the peak at 770 K was more pronounced than that of Ru/SiO_2-Al_2O_3. These results agreed with the BET results that the silica-alumina support had a character between these two other supports.

(b) TPD Profile of Oxygen

The TPD profiles of 5 percent oxygen at room temperature in helium on a series of ruthenium-gold supported on silica are shown in Figure 4.17. All
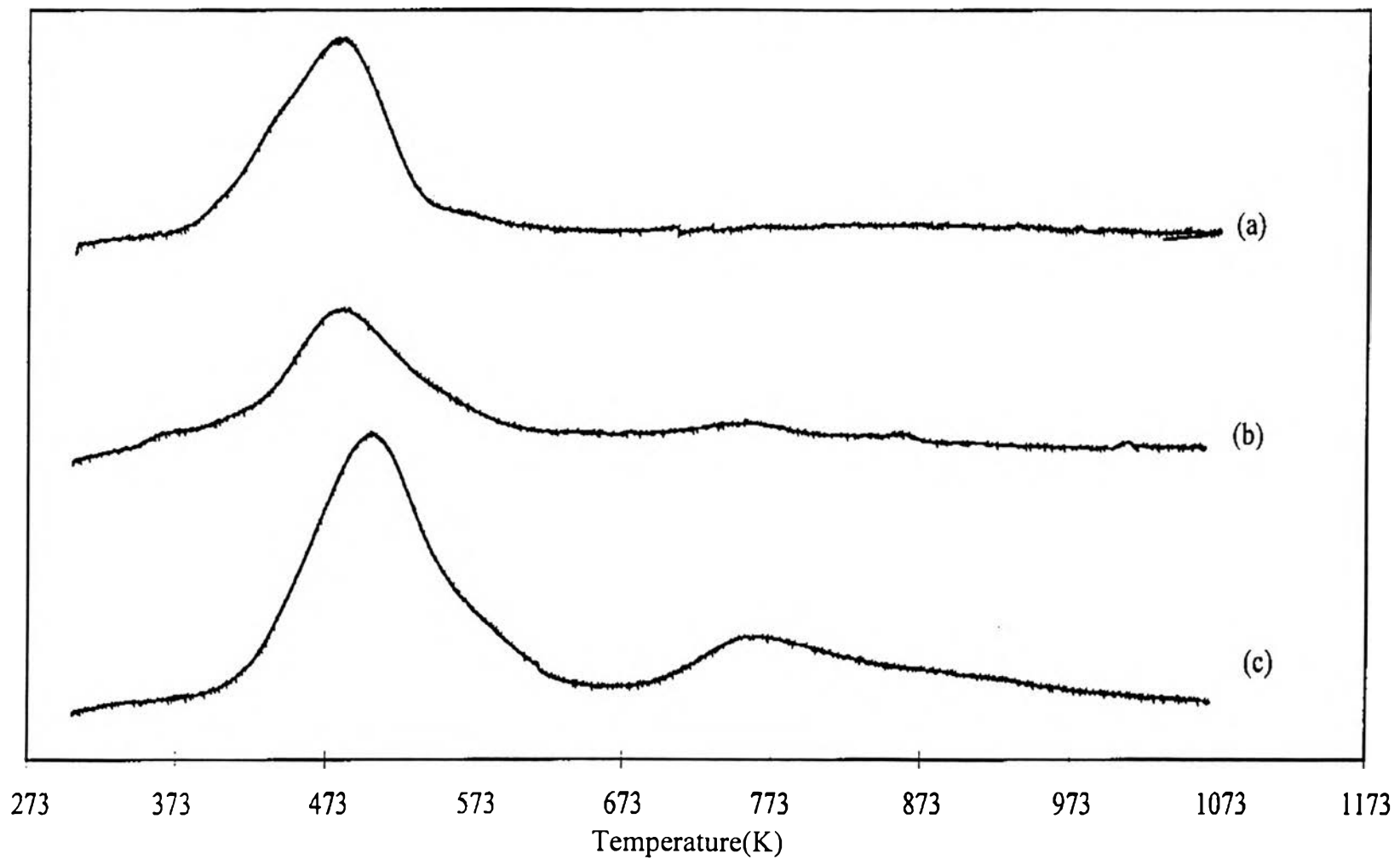
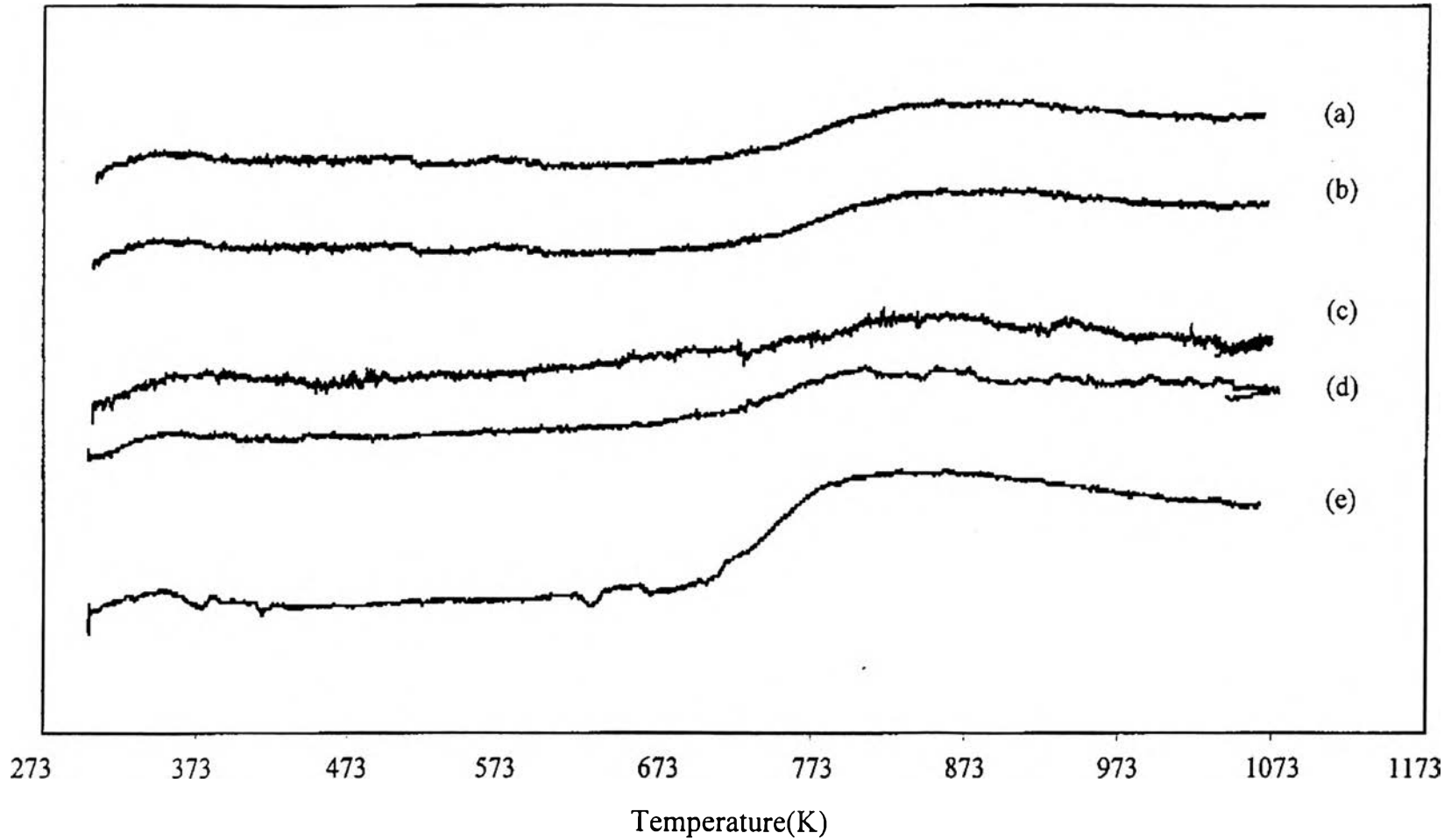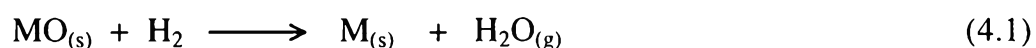Figure 4.16 Temperature-programmed desorption of methanol on (a)Ru/η-Al₂O₃ (b)Ru/SiO₂-Al₂O₃ (c)Ru/γ-Al₂O₃

Figure 4.17 Temperature-programmed desorption of 5%oxygen on (a)RS100 (b)RS091 (c)RS048 (d)RS014 (e)RS000

of the profiles looked quite similar. It was like a step change of signal at about 723 K. It implies that the desorption of oxygen occurred over a wide range of temperature or it may be possible that oxygen may readsorb on the catalyst sample or the energy of the surface sites was non-uniform. These results of TPD of oxygen agrees with the work of Choi *et al.* (1998) that adsorbed oxygen seemed to remain on the catalysts surface because oxygen TPD line did not return down to base line. Furthermore, as can be seen in Figure 4.18, TPD profiles of all catalysts mainly supported on alumina look the same but different on the silica-supported catalysts. There clearly were two broad peaks. However, the lines still did not return to base line. It can be explained that the adsorption and desorption of oxygen depend mainly on the support of catalysts.

(c) TPR Profile without Pretreatment with Oxygen

Figure 4.19 shows the TPR profiles of a series ruthenium-gold catalysts without pretreatment with oxygen. In all catalyst samples, there was a similar step change starting at about 600 K for RS048, RS091, and RS100, at about 500 K for RS014, and at about 700 K for RS000. This behavior did not occur on the catalysts having pretreatment with oxygen as shown in Figure 4.20. It might be because of the hydrogen spillover effect on silica support. Each peak in the TPR profiles indicates the consumption of hydrogen as in equation (4.1). Hydrogen can adsorb on silica which was not covered by oxygen. This behavior occurred at high temperatures because at high temperatures, most of water on silica surface is removed (Satterfield, 1991) causing hydrogen to adsorb easily on a silica.
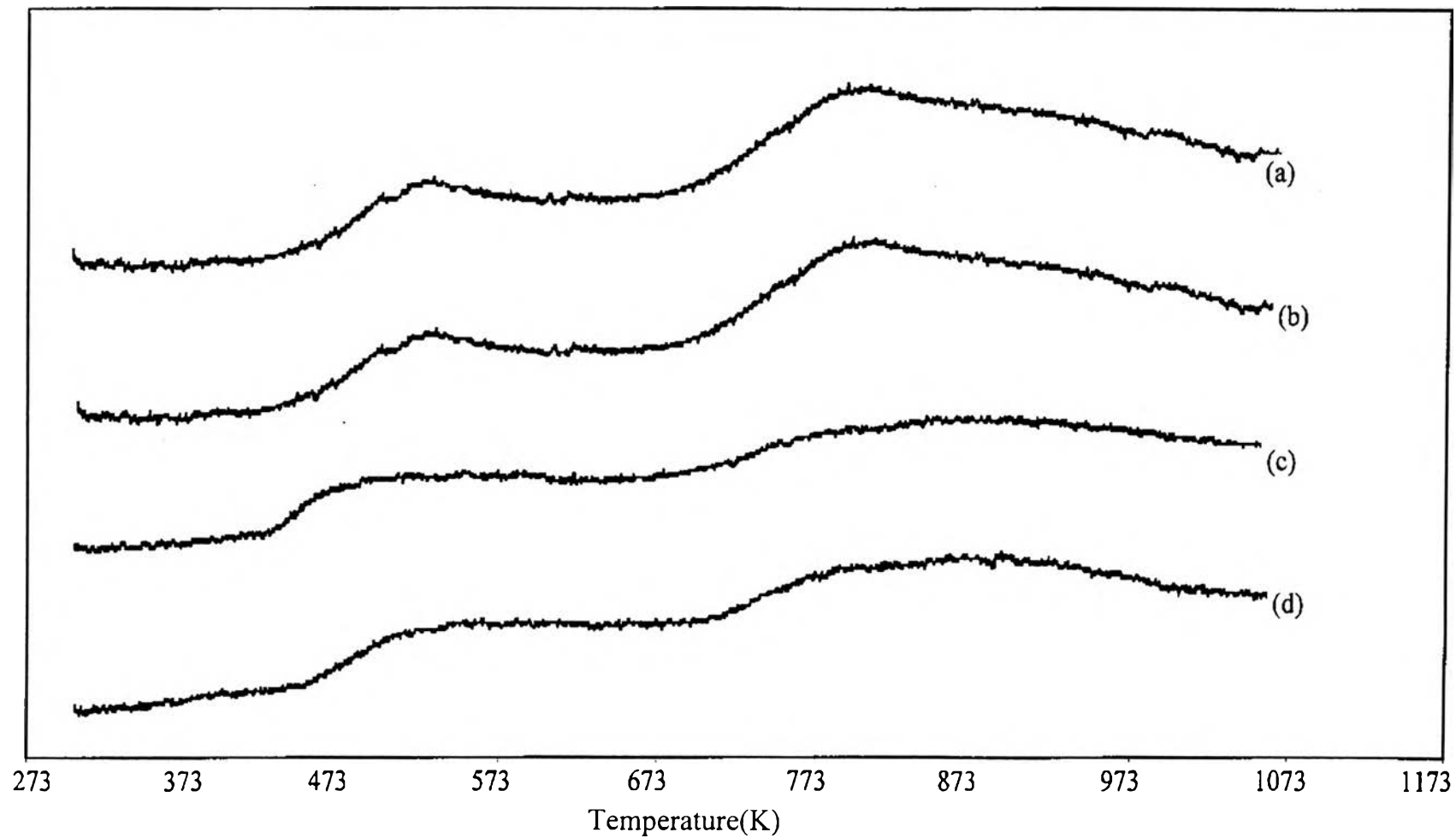
$$MO_{(s)} + H_2 \longrightarrow M_{(s)} + H_2O_{(g)} \tag{4.1}$$

Figure 4.18 Temperature-programmed desorption of 5%oxygen on (a)Ru/γ-Al₂O₃ (b)Ru/SiO₂-Al₂O₃ (c)Ru/η-Al₂O₃ (d)Ru-Au/η-Al₂O₃
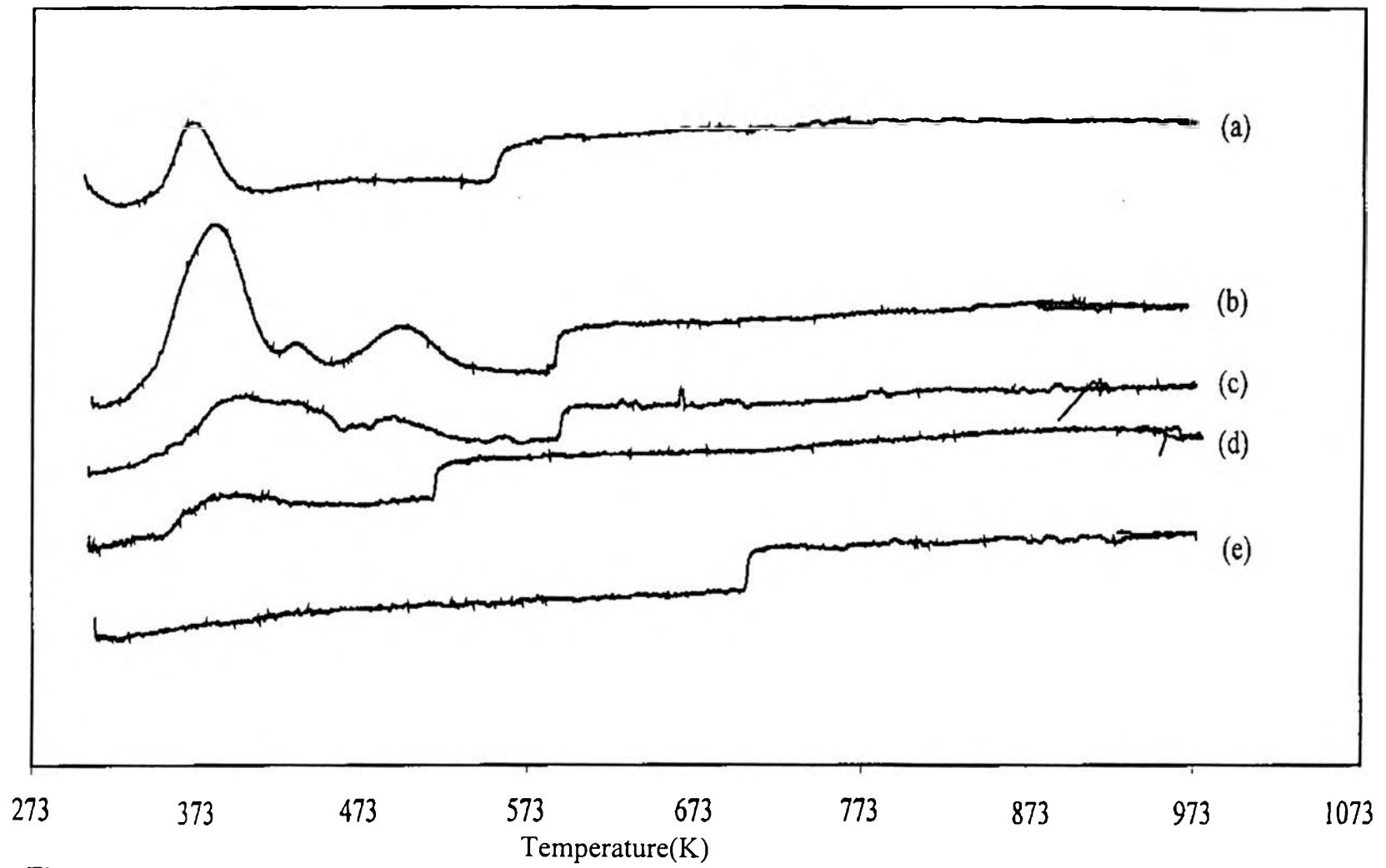
Figure 4.19 Temperature-programmed reduction on (a)RS100 (b)RS091 (c)RS048 (d)RS014 (e)RS000 without pretreatment with 5% oxygen
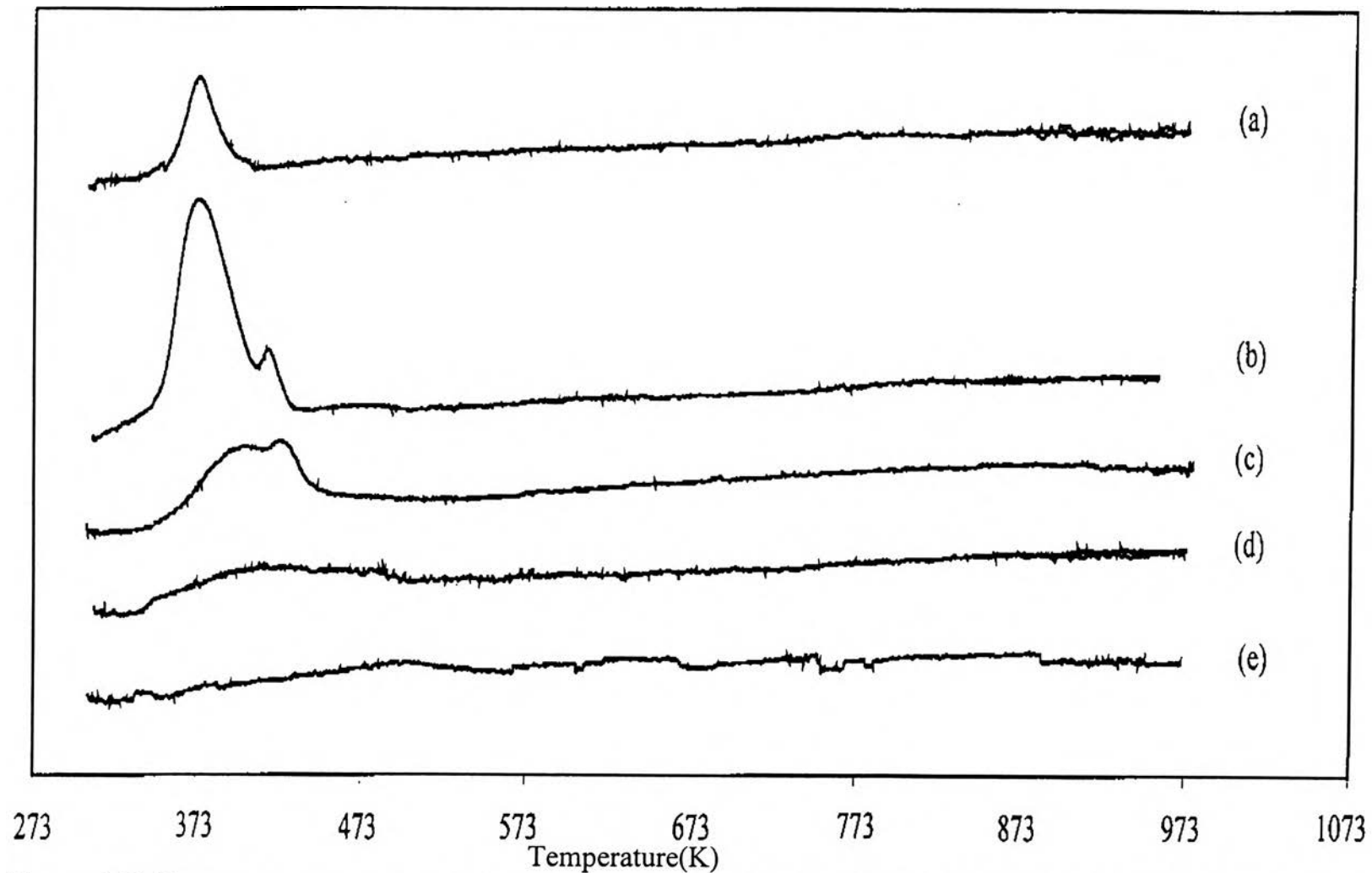
Figure 4.20 Temperature-programmed reduction on (a)RS100 (b)RS091 (c)RS048 (d)RS014 (e)RS000 pretreatment with 5% oxygen

There was only one peak on RS100 at 373 K corresponding to the ruthenium active site in ruthenium monometallic catalyst. For pure gold supported on silica, RS000, there was no gold active site observed on this catalyst. However, when gold was incorporated with ruthenium as bimetallic catalysts, there were more than one peak in RS048 and RS091. For RS091, there were three peaks at 384 K, 435 K, and 500 K. In contrast to RS091, the peaks of RS048 were not as well resolved. The spectrum was deconvoluted to three peaks at 400 K, 430 K, and 500 K. The peak of RS014 was not clearly resolved as well. It was a broad peak with low signal at 387 K. This might indicate the spillover phenomena of hydrogen. When gold was added to ruthenium catalysts, it assisted in the reduction of ruthenium metal depending on the gold content as well. From the spectrum of RS000, it showed that gold was difficult to be reduced. Ruthenium might assist gold to form metallic gold at high temperature with suitable gold content. This agreed with the work of Tauszik *et al.* (1984). They found that the peak at 490 K for RS062 and RS048 was simply a gold signal superimposed on ruthenium. The peak at 435 K might correspond to species deriving from an interaction between ruthenium and gold compounds which was evident from RS091 spectrum when the elements were present in suitable amounts. The reduction was shifted to a higher temperature by the presence of gold.

(d) TPR Profile with Pretreatment with Oxygen

The TPR profiles of a series ruthenium-gold bimetallic catalysts after pretreatment with 5 percent oxygen in helium are shown in Figure 4.20. All catalyst samples were exposed to 5 percent oxygen in helium at 673 K for 2 hours before running TPR because oxygen can chemisorb on supported gold at 673 K (Chang *et al.*, 1998). Clearly, the peaks were more pronounced than that of non-treated samples and the signal of step change disappeared in all

samples. In the low temperature region before the step-change, the results looked similar for RS000, RS014, and RS100 compared with non-pretreated samples. For RS048 and RS091, the third peak at about 500 K disappeared, and the reduction temperature of ruthenium was no longer shifted to higher temperature by the presence of gold in RS091. Tauszik *et al.* (1984) observed the TPR spectrum of pure $RuCl_3H_2O$ reducing at about 525 K. So this peak might be corresponding to the third peak that disappeared with pretreatment with oxygen just like one of the impurities. However, as it was mentioned before, that peak might be the peak of the gold signal. Certainly, the appearance of the peak at 430 K in RS091 was the species deriving from an interaction of ruthenium and gold. That peak was not clear in RS048 because the amount of two metals was not suitable.

Figure 4.21 shows the effect of support materials on TPR spectra. The silica-alumina support did not modify the active site in catalyst samples because there was no more active site created on this catalyst sample compared to that on both silica and alumina. The behavior was still compromised silica and alumina support behavior. This agrees with the surface area results.

4.2 Methanol Oxidation

The relation between methanol conversion and time at different temperature is shown in Figures 4.22-4.26 for a series of ruthenium-gold catalysts supported on silica. For all catalysts, time required for steady state was at around 200 min. The higher the reaction temperature was, the faster the steady state reached. At the higher temperature, the effects of heat transfer and pore diffusion are so significantly high that caused the conversion higher. At a high temperature, methanol conversion increased as a function of time and then leveled off. In contrast, at a low temperature, methanol conversion
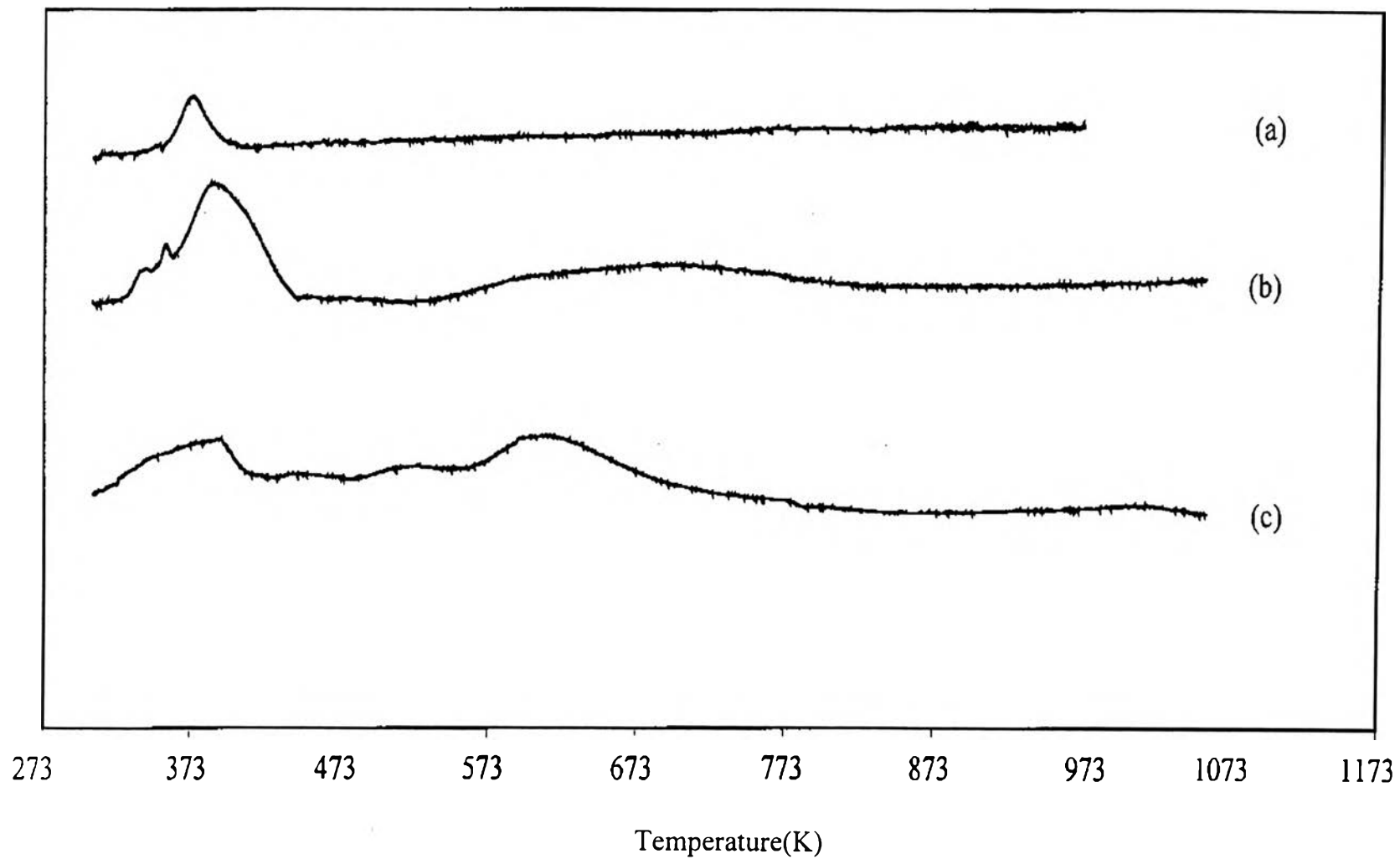
(a)

(b)

(c)

273   373   473   573   673   773   873   973   1073   1173

Temperature(K)

Figure 4.21 Temperature-programmed reduction on (a)Ru/SiO₂ (b)Ru/SiO₂-Al₂O₃ (c)Ru/γ-Al₂O₃

increased and then decreased until it was constant at the steady state time. This is because at the low temperature, it was only the chemical kinetic effect. The catalyst was fresh at the initial time so the conversion was higher than at the steady state. However, at the higher temperature, as mentioned before, there were the significant effects of mass and heat transfer or pore diffusion. The freshness of catalyst was rather not important in comparison with the temperature so that the conversion did not decrease as time.
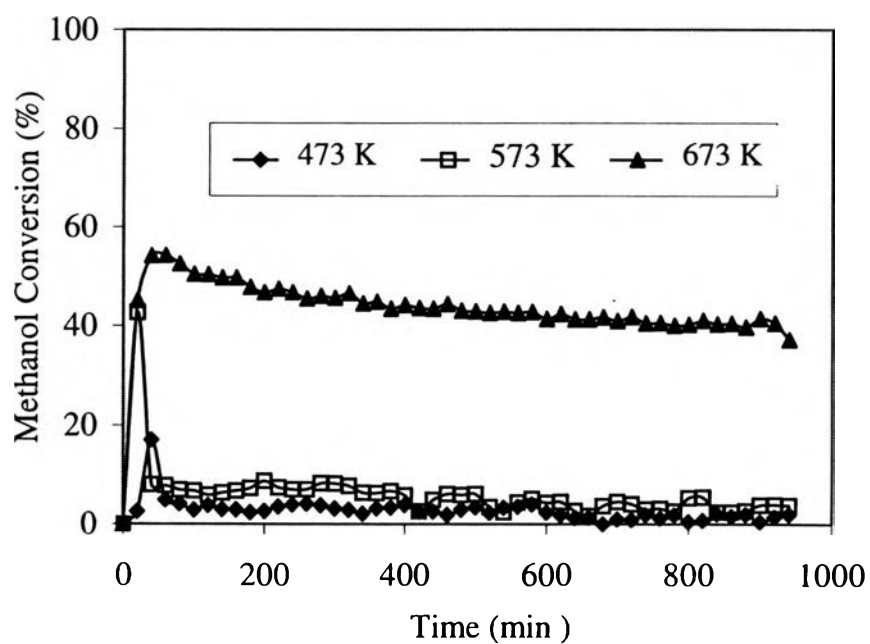
Figure 4.22 Methanol conversion as a function of time on RS000 at the different temperatures
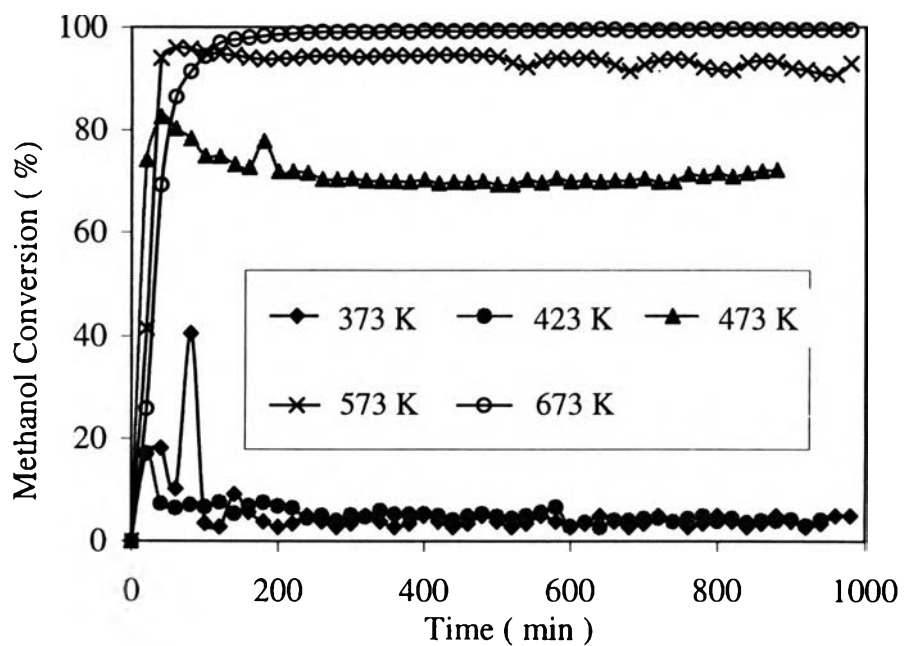
**Figure 4.23 Methanol conversion as a function of time on RS014
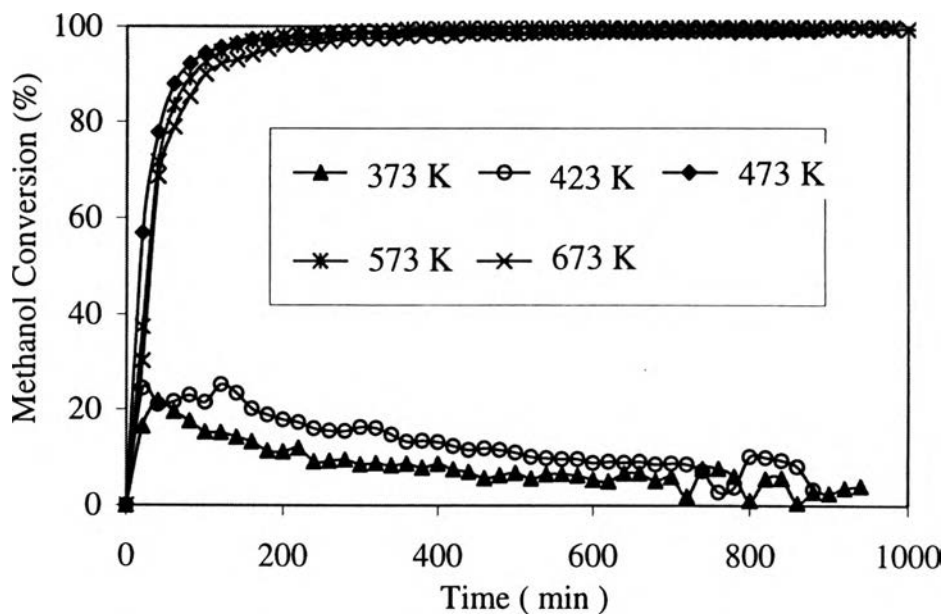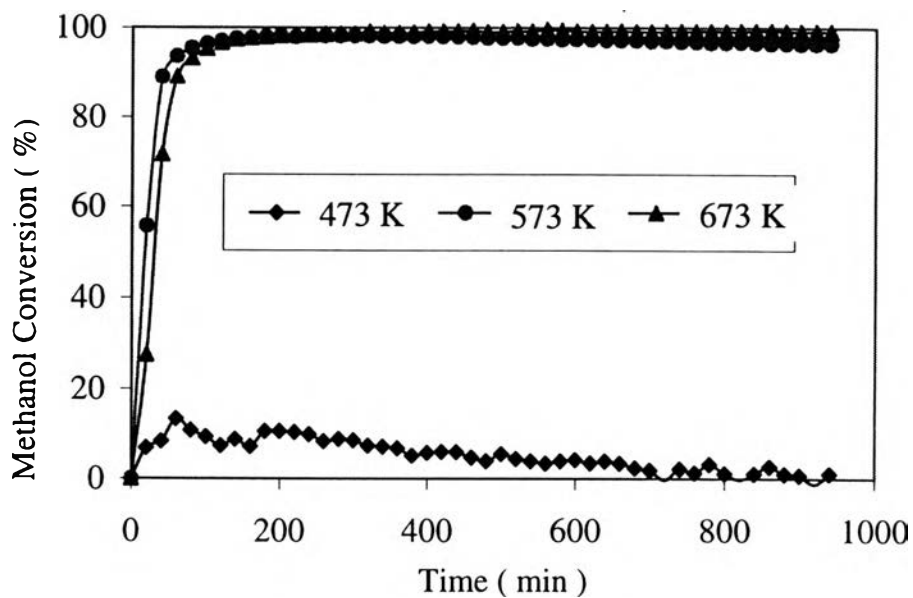at the different temperatures**
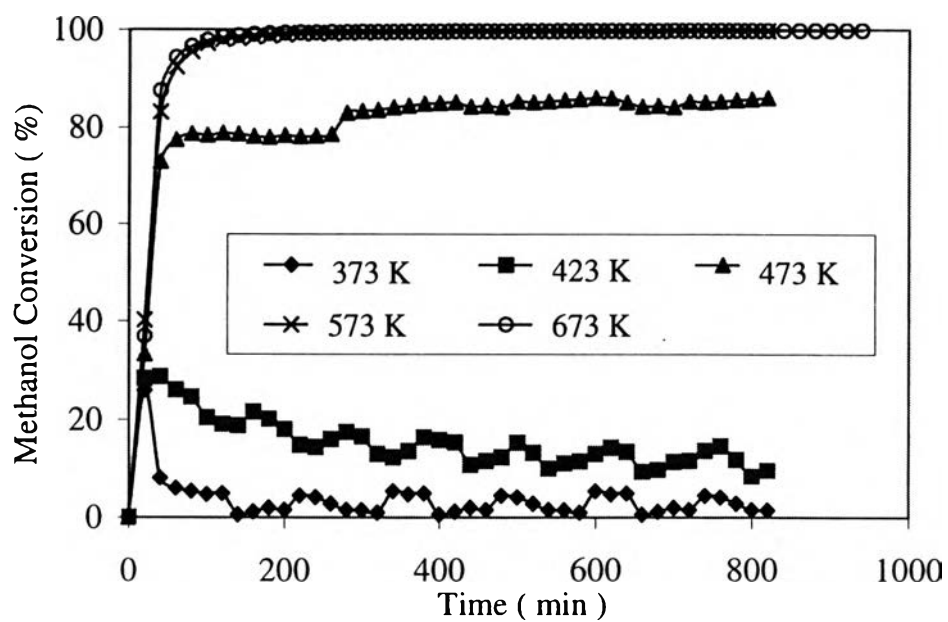
**Figure 4.24 Methanol conversion as a function of time on RS048
at the different temperatures**

**Figure 4.25 Methanol conversion as a function of time on RS091
at the different temperatures**

**Figure 4.26 Methanol conversion as a function of time on RS100
at the different temperatures**

Figure 4.27 shows the light-off temperature of methanol conversion on the silica-supported ruthenium catalysts. It shows the relation between the methanol conversion at the steady state and the reaction temperature. The temperature at which the conversion starts to rise steeply is called the light-off temperature. The temperature at which the conversion of reactant exceeds 50 % is usually denoted the light-off temperature (Törncrona *et al.*, 1997).
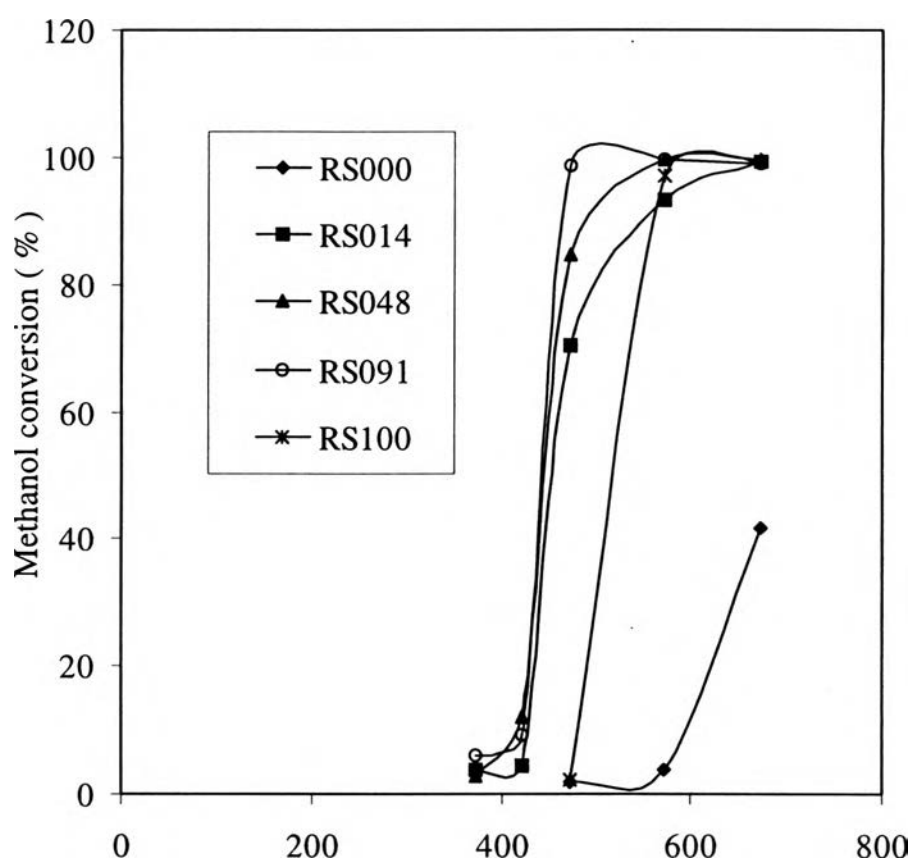
Figure 4.27 Light-off temperature of methanol conversion in methanol oxidation on the silica supported ruthenium catalysts

For this Figure, it is easy to see each effect for each range of temperatures. For the bimetallic catalysts, RS014, RS048, and RS091, the chemical kinetic reaction rate steps were in the temperature range of 373-423 K, pore diffusion steps of 423-573 K, and the bulk mass transfer of 573-673 K. The temperature for 50 % methanol conversion were decreased from 448, 440, and 435 K when the content of gold was decreased in RS014, RS048, and RS091 respectively. This decrease in temperature for the constant conversion was seen more obviously for the higher conversion as nearly bulk mass transfer steps at around 90% methanol conversion. The temperatures for 90% methanol conversion were 543, 483, and 458 K for RS014, RS048, and RS091 respectively. Moreover, below 40 % methanol conversion which was in the pore diffusion step range, the behavior of RS091 and RS048 was the same. However, the temperature during this low conversion for RS048 was a little bit lower than that for RS091. From all the results, an increase in gold content would increase the light-off temperature of these bimetallic catalysts except for pure ruthenium supported on silica (RS100). However, this behavior was changed in the bulk mass and heat transfer step at the temperature beyond 573 K. For RS000, this catalyst was so inert even at the highest reaction temperature (673K); the methanol conversion did not reach 50 %. It is explained that the light-off temperatures of each catalyst do not only depend on the reaction temperature range but also depend on the gold and ruthenium content. RS091 was the best catalyst among these three bimetallic catalysts, as confirmed with the TPR results that there was a new species derived from the two metals. This might be the active site for methanol oxidation, which was more active than ruthenium or gold site. However, in each region, chemical kinetics, pore diffusion, and bulk mass transfer, the behavior of each catalyst was different as well. These ruthenium catalysts might be of great candidate for the methanol oxidation. From the works of Ozkan *et al.* (1990), they observed the temperature required for 50 % methanol conversion at around

433 K for nonprecious oxide transition metal catalysts and from the work of Yang and Lunsford (1987), they found at around 573 K on molybdenum supported on silica. So the light-off temperatures of these bimetallic ruthenium catalysts studied can be comparable. The light-off temperatures for 50 %conversion for RS014, RS048, and RS091 were 448, 440, and 435 K as mentioned before.

It can not be concluded that this reaction is favored by either amorphous or crystalline materials. From the XRD results, the bimetallic catalysts were both amorphous and crystalline.

At a low reaction temperature below 423 K, there was no carbon dioxide detected, but methyl formate ($HCOOCH_3$) was detected for bimetallic catalysts. This finding is agreed well with the experimental results given by Elmi et al. (1989). They studied the oxidation of methanol and found methyl formate over vanadium-titanium oxide catalysts as shown in equation (4.2):

$$2CH_3OH + O_2 \longrightarrow HCOOCH_3 + 2H_2O \qquad (4.2)$$

Since no carbon monoxide was detected at a high temperature so that the reaction should be:

$$2CH_3OH + 3O_2 \longrightarrow CO_2 + 2H_2O \qquad (4.3)$$
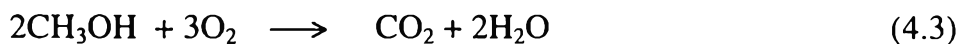
This is because of the excess oxygen in the reaction (VOC 1000 ppm, oxygen 21,000 ppm).

Figure 4.28 shows the Arrhenius plots of the oxidation of methanol on the bimetallic ruthenium-gold catalysts. The reaction rates were measured at the methanol conversion less than 15 % at which bulk and intraparticle mass transfer resistance was formed to be negligible. It is evident that RS014 gave similar reaction rate to RS091 because the activation energy (or the slope of

Arrhenius plots) was rather the same. The activation energy of RS091 was significantly lower than those of RS014, and RS048. The activation energy was lowest value for RS091 agreed with the light-off temperature that this catalyst was the best from these three bimetallic catalysts.
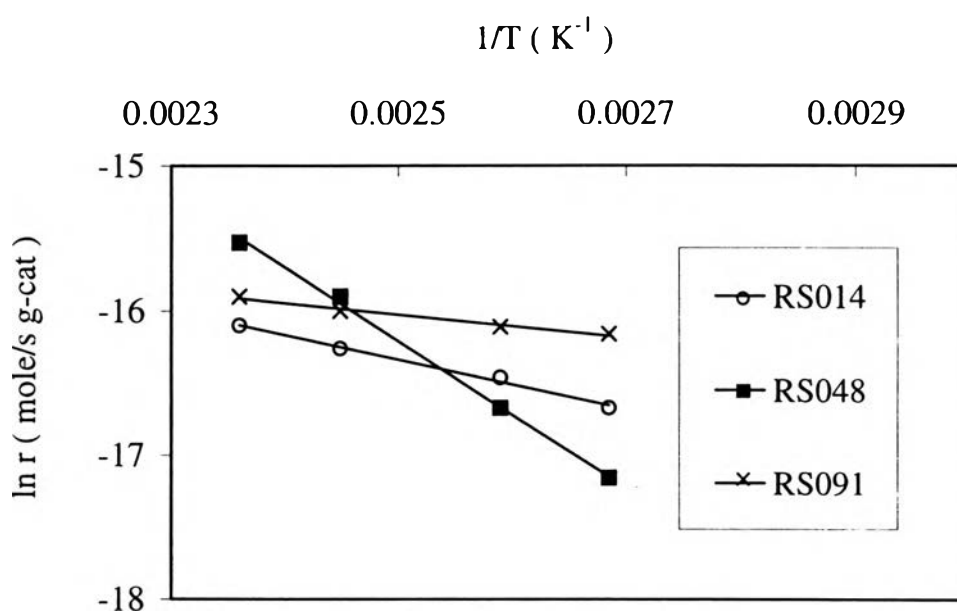

Figure 4.28 Arrhenius plots for the bimetallic ruthenium-gold catalysts

Figure 4.29 shows the influence of gold content and the reaction temperatures on the oxidation rate of methanol. At the low temperature of 473 K, when gold content increased, the rate increased until reached the maximum value at the gold content 20 atomic percentage and then gradually decreased. Beyond gold content of 80 atomic percentage, the oxidation rate declined drastically. This behavior did not occur at the high temperatures. At the high temperatures of 573 and 673 K, there were significant effects of both bulk

transfer and pore diffusion so the effect of catalysts was not important. The influence of gold content in catalysts did not affect the rate much.
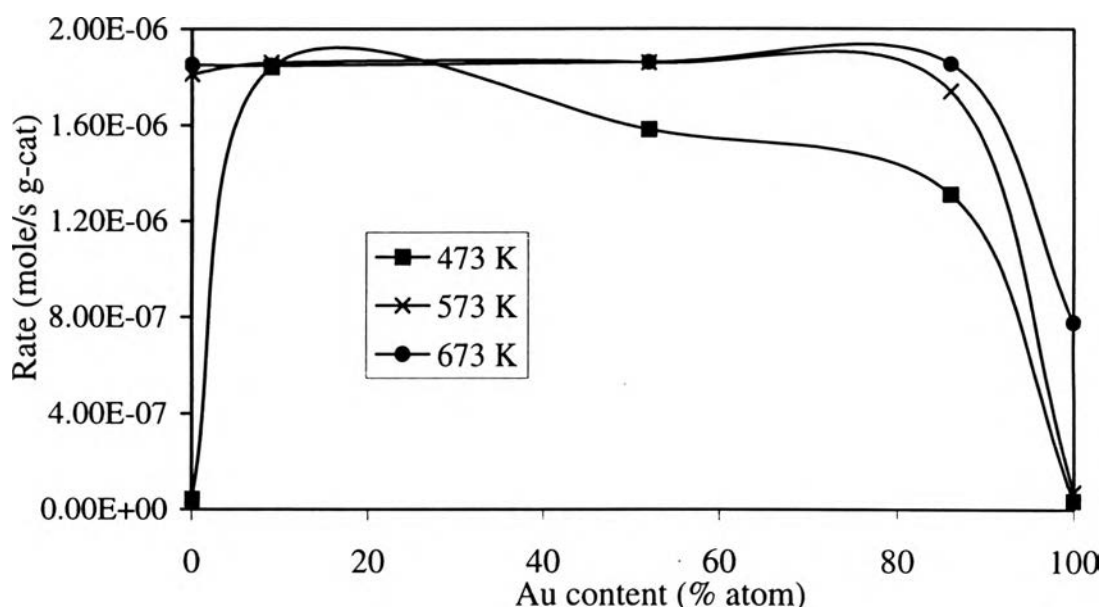
Figure 4.29 The rate of methanol oxidation on mono-and bimetallic Ru catalysts as a function of Au content in atomic percent

The XRD patterns for all catalysts supported on silica after methanol oxidation are shown in Figure 4.30. The sharp peak at around $28°(2\theta)$ was found in all catalysts composing of ruthenium element (RS014, RS048, and RS091) but it did not found in fresh catalysts as shown in Figure 4.13. It is simply drawn a conclusion that ruthenium in bimetallic clusters was oxidized to RuO_2 after methanol oxidation. This peak was found even in pure ruthenium supported on silica (RS100). For RS000, after reaction, the peaks at 78 and 82 $°(2\theta)$ disappeared because these five peaks were the peaks of pure gold. After reaction, the gold crystal might be destroyed or changed to other form so those two peaks disappeared. However, the bimetallic crystals were still active. The peaks of bimetallic species before and after reaction were the same for RS014, RS048, and RS091.
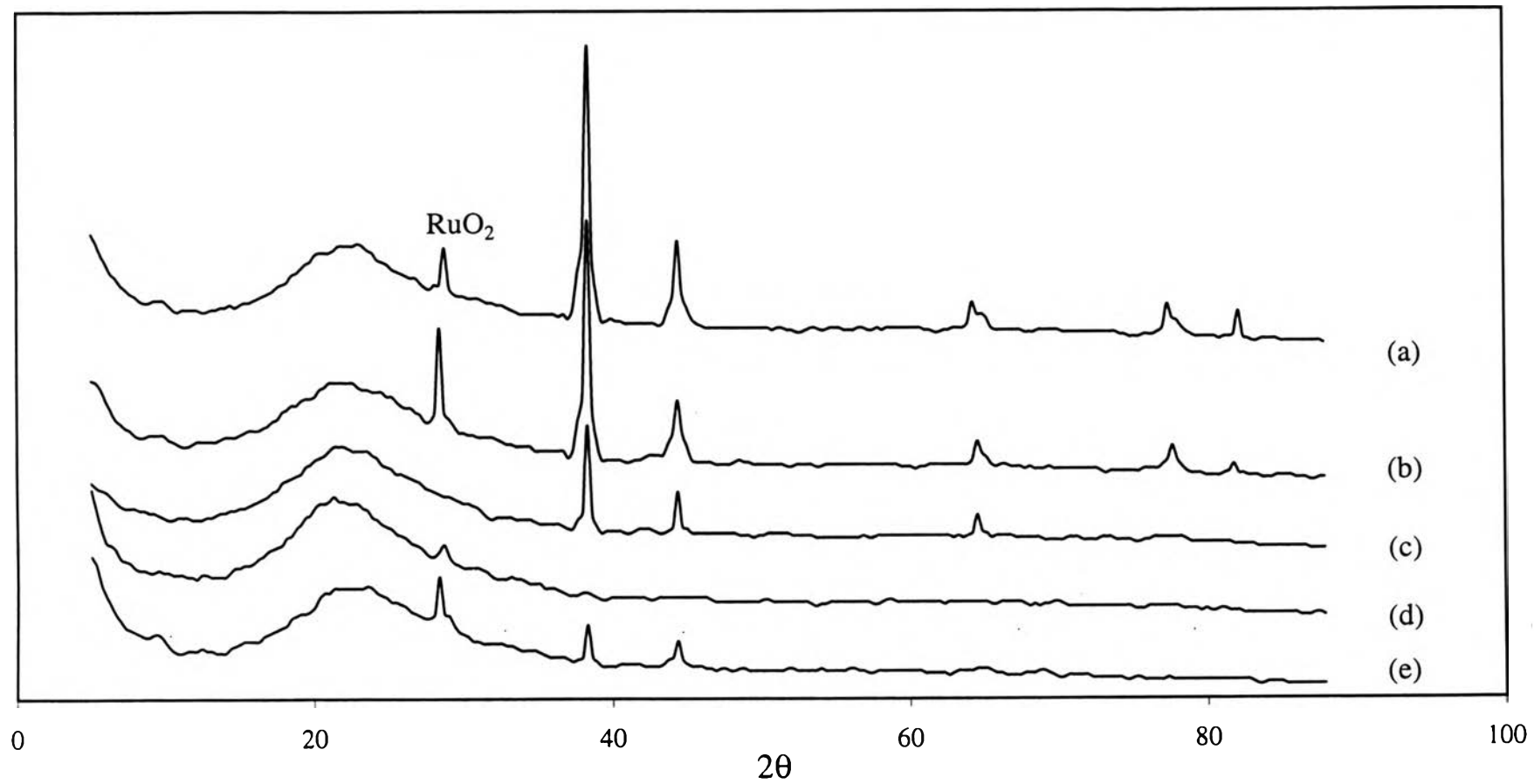
Figure 4.30 XRD patterns after methanol oxidation of (a) RS014 (b) RS048 (c) RS000 (d) RS100 (e) RS091

The effect of support material on methanol oxidation is shown in Table 4.3. The addition of gold in ruthenium supported on η -Al₂O₃ did not increase the methanol conversion but decreased the methanol conversion significantly. This agreed with the characterization part that the bimetallic clusters did not form on the alumina support. However, the methanol conversion observed on both γ-Al₂O₃ and SiO₂-Al₂O₃ support was relatively higher than that observed on silica support. It might be because methanol decomposed on both γ-Al₂O₃ and SiO₂-Al₂O₃ support or it was oxidized to the other substances. It is confirmed by the GC analysis results showing several peaks in the FID patterns. The products found were not only CO_2 and methyl formate but also the other substances. It might be formic acid, dimethyl ether or formaldehyde. Any way, it was still the oxygenated compounds, which were not the environmental friendly substances.

Table 4.3 The methanol conversion observed at 473 K on the different support ruthenium catalysts

Catalyst Sample	Methanol Conversion, %
Ru-Au/η-Al₂O₃	30.91
Ru/η-Al₂O₃	91.99
Ru/SiO₂-Al₂O₃	99.43
Ru/γ-Al₂O₃	99.57